

A multi-scale analysis of the crystallization of amorphous germanium telluride using ab initio simulations and classical crystallization theory

Jie Liu, Xu Xu, Lucien Brush, and M. P. Anantram

Citation: Journal of Applied Physics **115**, 023513 (2014); doi: 10.1063/1.4861721
View online: http://dx.doi.org/10.1063/1.4861721
View Table of Contents: http://scitation.aip.org/content/aip/journal/jap/115/2?ver=pdfcov
Published by the AIP Publishing



[This article is copyrighted as indicated in the article. Reuse of AIP content is subject to the terms at: http://scitation.aip.org/termsconditions. Downloaded to] IP: 128.95.215.110 On: Wed, 15 Jan 2014 22:18:00

A multi-scale analysis of the crystallization of amorphous germanium telluride using *ab initio* simulations and classical crystallization theory

Jie Liu,[1] Xu Xu,[1] Lucien Brush,[2] and M. P. Anantram[1]
[1]*Department of Electrical Engineering, University of Washington, Seattle, Washington 98195, USA*
[2]*Department of Material Science and Engineering, University of Washington, Seattle, Washington 98195, USA*

(Received 15 October 2013; accepted 24 December 2013; published online 10 January 2014)

The crystallization properties of the prototypical binary phase change material (PCM) germanium telluride (GeTe) are investigated by combining crystallization theory with *ab initio* molecular dynamics simulations. The temperature dependence of the physical quantities that determine the crystallization properties is calculated and analyzed. It is shown that the critical nucleus radius of a crystalline cluster is smaller than 1.4 nm when the annealing temperature is lower than 600 K, indicating an extremely promising scaling scenario. Our analysis reveals that the elastic energy, which is largely ignored in existing PCM crystallization studies, plays an important role in determining various crystallization properties and the ultimate scaling limit of the PCM. By omitting the influence of elastic energy, the critical formation energy (critical nuclei radius) will be underestimated by 41.7% (22.4%), and the nucleation rate will be overestimated by 74.2% when the annealing temperature is 600 K. © *2014 AIP Publishing LLC*.
[http://dx.doi.org/10.1063/1.4861721]

I. INTRODUCTION

The chalcogenide phase change materials (PCMs) play a crucial role in non-volatile optical and electrical information storage device technologies. In both optical and electrical PCM-based devices, the information is stored via rapid and reversible changes between the crystalline phase (*c*-) and the amorphous phase (*a*-) of the PCM. The stored data can be read out by taking advantage of the large contrast of optical reflectivity or electrical resistivity between the two phases.[1–3]

It has been found that the chalcogenide PCMs possess many interesting, rare, and useful physical properties.[1–15] First, both the crystalline phase and the amorphous phase PCM can be kept stable for a long time (10^1 years) without external power supply, making the PCM devices ideal for non-volatile memory applications.[1–3] Second, the PCM technology has superb scalability. Now, it is known that the PCM scaling can significantly improve the device speed, endurance, and stability.[3] The scaling experiments have shown that the bulk crystallization temperature can be kept when the PCM is scaled to 2 nm (Ref. 8), and the phase change properties can be kept in sub-2 nm PCM nanostructures.[9,10] The superb scalability of PCM is very useful to enable next-generation ultra-dense data storage technology. Third, the PCM devices can be designed to be very energy efficient. Experiments have shown that the operation of the PCM device can be accomplished using only single fJ energy,[5] making it suitable for low-power information storage applications. Fourth, the phase change of PCM is extremely fast. Recent research has shown that the PCM devices can finish the phase transition within only 0.5 ns, making the PCM technology promising in high speed electronic applications. These findings have spurred intensive interest in developing a theoretical understanding of the microscopic origin of the PCM's unique physical properties.[7,16–28] They also have invoked extensive research efforts focused on the implementation of PCMs into next-generation ultra-fast and ultra-dense non-volatile information storage devices.[1–3] Using *ab initio* simulations, a lot of insights have been obtained about the amorphization process,[16,18,19,25,27] crystallization process,[7,21,28] and electronic and lattice structure[17,19,20,22–28] of PCM.

The fast phase-change speed and the high scalability of PCMs largely hinge on the unique crystallization properties of the *a*-PCM. So it is important to investigate the crystallization behavior of the *a*-PCM, in order to glean deeper scientific understanding and to search for better material stoichiometry that will enable faster and more scalable information storage technologies. Although the crystallization of *a*-PCM has been extensively studied, detailed knowledge of the roles of different physical mechanisms controlling the crystallization properties remains unclear. In this paper, we investigate the temperature-dependent crystallization properties of a prototypical binary PCM germanium telluride (GeTe) alloy compound by combining classical nucleation and growth theory with *ab initio* simulations. The physical effects (atomic diffusion, Gibbs free energy differences, elasticity and interfacial energies) that govern the crystallization process are quantitatively analyzed. In Sec. II, the *ab initio* simulation procedure and the nucleation and growth theory are introduced. In Sec. III, simulation results are presented and analyzed. In Sec. IV, we discuss the technological implications of the results presented in this paper.

II. MODELING METHODOLOGY

A. Classical crystallization theory

It has been experimentally observed that the crystallization of *a*-GeTe, like most crystallization processes, occurs in two-stages: (1) thermally activated homogeneous nucleation occurring inside the *a*-GeTe to form small crystalline clusters and (2) the continued growth of the crystalline clusters

 © 2014 AIP Publishing LLC

[This article is copyrighted as indicated in the article. Reuse of AIP content is subject to the terms at: http://scitation.aip.org/termsconditions. Downloaded to] IP: 128.95.215.110 On: Wed, 15 Jan 2014 22:18:00

beyond the nucleation stage at the expense of the parent *a*-GeTe phase. The growth is driven by the continued decrease in the system free energy as equilibrium is approached. In the GeTe case, the growth rate is controlled by the molecular processes occurring at the interface separating *a*-GeTe from *c*-GeTe.[1]

According to classical crystallization theory,[29] the nucleation of *a*-GeTe can be represented by a fictitious three-step operation at constant temperature (T) and pressure (P): (1) the removal of a small volume of *a*-GeTe from the bulk phase followed by unconstrained transformation into *c*-GeTe, (2) the application of a surface traction to the *c*-GeTe that deforms the product phase to its original untransformed volume followed by its insertion back into the void formed by evacuating the small volume of *a*-GeTe (the mass density of the *c*-GeTe is larger than that of the *a*-GeTe), and (3) relaxation of the reinserted volume of *c*-GeTe and the surrounding *a*-GeTe. The energy changes associated with these three steps provide three components of the crystalline cluster formation energy ΔG

$$\Delta G = \frac{4}{3}\pi r^3 \Delta G_{ac} + \frac{4}{3}\pi r^3 E_e + 4\pi r^2 \sigma, \tag{1}$$

where r is the effective radius of the crystalline cluster seed of *c*-GeTe, $\Delta G_{ac} = G_c - G_c$ is the volume free energy change associated with the formation of *c*-GeTe from *a*-GeTe, G_c (G_a) is the Gibbs free energy of the *c*-GeTe (*a*-GeTe), E_e is the elastic energy of the *c*-GeTe, and σ is the energy of the *a*-GeTe/*c*-GeTe interface (assumed isotropic). As schematically shown in Fig. 1(a), a particle nucleates by overcoming its critical formation energy ΔG_c.

Typically many particles will nucleate during a crystallization process. The nucleation rate I can be approximated by an Arrhenius law

$$I = I_0 e^{-\frac{E_D + \Delta G_c}{kT}}, \tag{2}$$

providing a number of nuclei forming per unit volume of parent phase, per unit time. Here, E_D is given by the energy barrier E_1 shown in Fig. 1(b), T is temperature, k is the Boltzmann constant, and I_0 is a prefactor.

A particle enters the growth stage once the effective radius of the *c*-GeTe cluster becomes larger than the critical nuclei radius r_c, as shown in Fig. 1(a). The growth of the *c*-GeTe is controlled by atomic processes occurring at the interface and not by long-range heat transport. Therefore, the growth of the *c*-GeTe is a consequence of two counter-balancing molecular-scale processes occurring across the interface: (1) atom transfer from amorphous to crystalline phase; and (2) atom transfer from crystalline to amorphous phase. The energy barriers for these processes are E_1 and $E_1 + E_2$ respectively, as shown in Fig. 1(b). Since the crystallization of *a*-GeTe is a thermally activated, trans-interfacial diffusion-limited process, $E_1 = E_D$ and $E_2 = \Delta G_{ac}$, where E_D is the activation energy for atomic diffusion in *a*-GeTe.[1,29]

Thus, the growth speed of the interface u is

$$u = u_0 e^{-\frac{E_D}{kT}}\left(1 - e^{-\frac{\Delta G_{ac}}{kT}}\right), \tag{3}$$

where u_0 is a prefactor.[1,29]

B. Simulation models

In order to obtain the quantitative values of the physical quantities described in Sec. II A, three models are created using canonical ensemble (NVT) *ab initio* simulations: (1) the *c*-GeTe model, (2) the *a*-GeTe model, and (3) the interface model.

The *c*-GeTe model contains 192 atoms. The supercell volume $V_c = L_x \times L_y \times L_z^c$ (upper case V and L mean fixed value) is chosen such that the mass density is the same as the measured value 6.06 g/cm^3.[30] The lattice structure of the measured rhombohedral *c*-GeTe (Ref. 31) is used to generate the atomic coordinates, which are relaxed using a conjugate gradient (CG) algorithm.

The *a*-GeTe model, which also contains 192 atoms, is obtained from a melt-quench *ab initio* molecular dynamics (AIMD) simulation model.[15] First, the *c*-GeTe model is melted at 2000 K for 7 ps and then brought down to 1000 K for 3 ps, in order to destroy the crystalline lattice structure and generate liquid phase (*l*-) GeTe. Then, the *l*-GeTe is quenched to 300 K over a 20 ps time interval. After the CG relaxation, the *a*-GeTe model is obtained. In the melt-quench AIMD simulations, the supercell volume is chosen as $V_a = L_x \times L_y \times L_z^a$ such that the mass density is the same as the measured value of 5.60 g/cm^3 observed for *a*-GeTe.[30] The pair distribution function (PDF) of the *a*-GeTe model obtained from the melt-quench AIMD simulations agrees well with the experimental measurement, as shown in our previous work.[15] The inter-atomic first and second nearest neighbor distances of the *a*-GeTe model are calculated to be 2.8 Å and 4.1 Å, which are in reasonable agreement with experimentally measured values of 2.7 Å and 4.2 Å, respectively.[32,33]

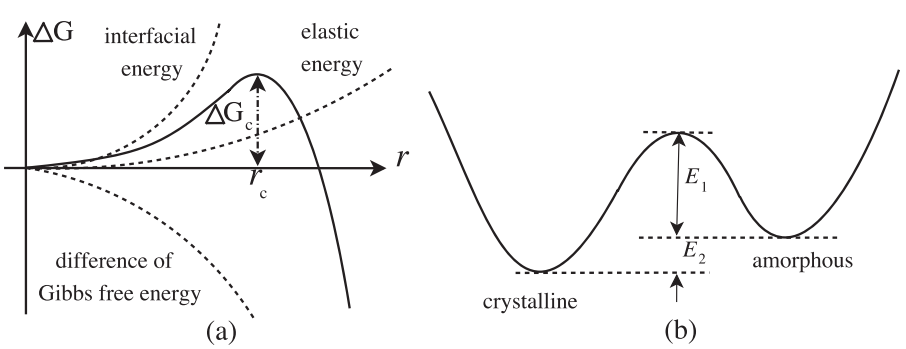


FIG. 1. Schematic energy barriers for (a) nucleation and (b) growth (ΔG is the formation energy, r is the effective radius of crystalline nuclei, ΔG_c is the critical formation energy, r_c is the critical radius, $E_1 = E_D$ activation energy for atom diffusion, and $E_2 = \Delta G_{ac}$ is the Gibbs free energy difference between *a*-GeTe and *c*-GeTe).

[This article is copyrighted as indicated in the article. Reuse of AIP content is subject to the terms at: http://scitation.aip.org/termsconditions. Downloaded to] IP: 128.95.215.110 On: Wed, 15 Jan 2014 22:18:00

The interface model, which contains 384 atoms, is created by putting the *c*-GeTe model and the *a*-GeTe model together in a supercell with volume $V_{ac} = L_x \times L_y \times (L_z^a + L_z^c)$ and then allowing CG relaxation. These three models will be used as the initial atomic coordinates for the following AIMD simulations.

C. *Ab initio* simulations

Isothermal-isobaric ensemble (NPT) AIMD simulations are performed on the three simulation models. Since the simulation supercell size is very small, the AIMD annealing temperature T is maintained at a uniform value using the Nose thermostat.[34] The Parrinello-Rahman method[35] maintains a vacuum by adjusting the supercell volume *in situ*. This procedure allows calculation of the temperature dependence of the mass density. The supercell volumes of the *c*-GeTe model, the *a*-GeTe model, and the interface model are $v_c = l_x \times l_y \times l_z^c$, $v_a = l_x \times l_y \times l_z^a$, and $v_{ac} = l_x \times l_y \times l_z^{ac}$, respectively (lower case v and l mean variable values). The AIMD simulations run for 8 ps, and the time-averaged temperature-dependent internal energies are shown in Fig. 2. Here, the simulation time is chosen to be long enough that the energy fluctuations are averaged out over time, but is short enough to prevent the phase change from *a*-GeTe to *c*-GeTe, which needs more than 10^2–10^3 ps.[1–3]

D. Simulation parameters

The *ab initio* simulations presented in this paper are performed using the density functional theory (DFT) package SIESTA.[36] At the supercell boundaries, periodic boundary conditions (PBCs) are applied. In the simulations, the AIMD time step is chosen to be 5 fs, the Gamma point is used to sample the Brillouin zone, the plane wave cutoff is chosen to be 100 Ry, the generalized gradient approximation (GGA) of Perdew, Burke, and Ernzerhof (PBE) is used to approximate the exchange-correlation energy,[37] the double-zeta plus polarization pseudo-atomic orbitals (PAO) is used for Ge and Te atoms, and the CG relaxation convergence criteria is set at 40 meV/Å.

III. SIMULATION RESULTS

In this section, the results obtained from *ab initio* simulations are presented. First we establish good agreement between the calculated mass density and specific heat capacity with experimental measurements. Then, atomic diffusion in *a*-GeTe is investigated. Finally, based on the simulation of the three components denoted in Eq. (1) (the Gibbs free energy, the elastic energy and the interfacial energy), the nucleation, and growth kinetics are calculated as a function of temperature.

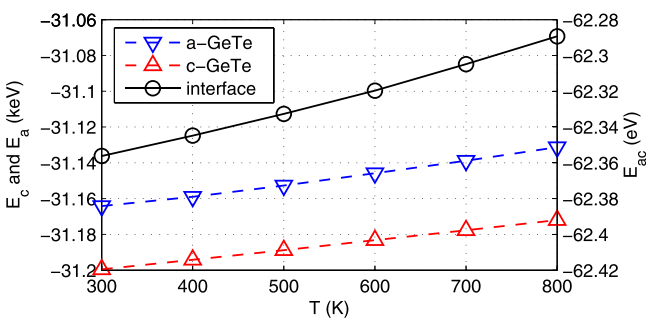


FIG. 2. Time-averaged temperature dependent internal energies of the *c*-GeTe model (E_c), the *a*-GeTe model (E_a), and the interface model (E_{ac}).

A. Mass density

In the NPT AIMD simulations introduced in Sec. II A, the volume of the supercell is allowed to change so that the internal pressure is maintained to be roughly zero. This allows us to calculate the temperature-dependent mass densities of *a*-GeTe (ρ_a) and *c*-GeTe (ρ_c), as shown in Fig. 3. The simulated ρ_a agrees well the measured value 5.60 g/cm^3; the simulated ρ_c/ρ_a values vary from 6% to about 9% over a five hundred degree range of temperature. Typical experimental measurements suggest that the mass density of the *c*-GeTe is about 8% higher than that of the *a*-GeTe,[1,30] which falls within the bounds of our calculations and, moreover, is within two percent agreement over the entire temperature range.

B. Specific heat capacity

The specific heat capacity of *a*-GeTe (*c*-GeTe) can be computed using the definition

$$c_{a(c)} = \left(\partial U_{a(c)}/\partial T\right)_P, \tag{4}$$

where T is the annealing temperature; $U_{a(c)} = E_{a(c)}/v_{a(c)}$ is the internal energy density; $E_{a(c)}$ is the internal energy (as shown in Fig. 2); and $v_{a(c)}$ is the supercell volume of the *a*-GeTe (*c*-GeTe) model.

Our simulation shows that $c_c = a_c + b_c T$, where $a_c = 1.45 \times 10^6$ J/Km^3 and $b_c = 292$ J/m^3, which are close to the experimentally measured values $a_c = 1.35 \times 10^6$ J/Km^3 and $b_c = 351$ J/m^3.[38] This means that when $T = 600$ K, the simulation result is $c_c = 1.62 \times 10^6$ J/Km^3, which is in decent agreement with the measured value 1.56×10^6 J/Km^3.[38] While the measured value of c_a is not available, we obtained $c_a = a_a + b_a T$ ($a_a = 1.11 \times 10^6$ J/Km^3 and $b_a = 1.51 \times 10^3$ J/m^3) using *ab initio* simulations, as shown in Fig. 4.

The specific heat capacity depends on the degrees of freedom (DOF) available in the material to store energy. It can be seen from Fig. 4 that at low temperature, c_a is slightly larger but comparable to c_c. As temperature increases, c_a becomes much larger than c_c because b_a is larger than b_c. Therefore, by increasing the annealing temperature, *a*-GeTe can enable more DOF than *c*-GeTe due to differences in lattice structure and chemical bonding.

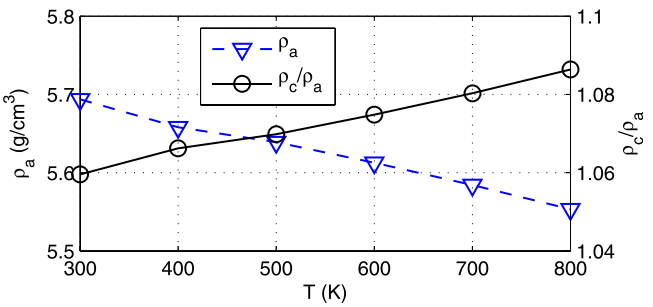


FIG. 3. Temperature dependent mass density.

[This article is copyrighted as indicated in the article. Reuse of AIP content is subject to the terms at: http://scitation.aip.org/termsconditions. Downloaded to] IP: 128.95.215.110 On: Wed, 15 Jan 2014 22:18:00

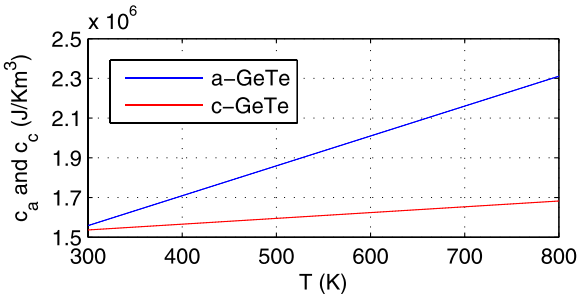


FIG. 4. Temperature dependent specific heat capacity of *a*-GeTe (c_a) and *c*-GeTe (c_c).

It should be noted that while c_c can be measured, it would be difficult to experimentally measure c_a, due to the nanosecond-scale *a*-GeTe to *c*-GeTe phase-change speed. Fortunately, the picosecond-level AIMD simulations can be used to obtain c_a. The specific heat capacity can influence the crystallization of *a*-GeTe via a difference in entropy that will be calculated in Sec. III D.

C. Diffusivity

The diffusivity of atoms in *a*-GeTe can be calculated using

$$D \approx \frac{1}{6t}\langle|\boldsymbol{r}_i(t) - \boldsymbol{r}_i(0)|^2\rangle, \tag{5}$$

where $\boldsymbol{r}_i(t)$ is the position of atom i (at time t) obtained from the AIMD simulations. The results of the mean square displacement (MSD) $\langle|\boldsymbol{r}_i(t) - \boldsymbol{r}_i(0)|^2\rangle$ for $T = 800$ K are shown in Fig. 5. The temperature dependence of the diffusivities of elemental Ge and Te in *a*-GeTe is shown in Fig. 6. Since diffusion is a thermally-activated process, the diffusivity obeys an Arrhenius law

$$D = D_0 e^{-\frac{E_D}{kT}}, \tag{6}$$

where D_0 is a prefactor and E_D is the activation energy. Using Eq. (6) and the values of D shown in Fig. 6, we can compute $E_D = 0.30$ eV for Ge atoms, $E_D = 0.32$ eV for Te atoms, and $E_D = 0.31$ eV for *a*-GeTe.

D. Gibbs free energy

As schematically shown in Fig. 1(b), *a*-GeTe is a metastable structure, the Gibbs free energy density of which (G_a) is higher than that of the *c*-GeTe (G_c). The difference between G_a and G_c can be calculated using

$$\Delta G_{ac} = \Delta U_{ac} - T\left(\frac{\Delta H_m}{T_m} + \int_{T_m-}^{T} \frac{c_a - c_c}{T} dT\right), \tag{7}$$

where $\Delta U_{ac} = U_a - U_c$; $U_{a(c)}$ is the internal energy density of *a*-GeTe (*c*-GeTe), $T_m = 998$ K is the melting temperature of GeTe,[1] $\Delta H_m = 1.45$ GJ/m^3 is the latent heat of fusion,[39] $c_{a(c)}$ is the specific heat capacity of *a*-GeTe (*c*-GeTe) as shown in Fig. 4. In Eq. (7), the terms inside the parenthesis represents $\Delta S_{ac} = S_a - S_c$, where $S_{a(c)}$ is the entropy density of the *a*-GeTe (*c*-GeTe). The simulation results for ΔG_{ac} are presented in Fig. 7.

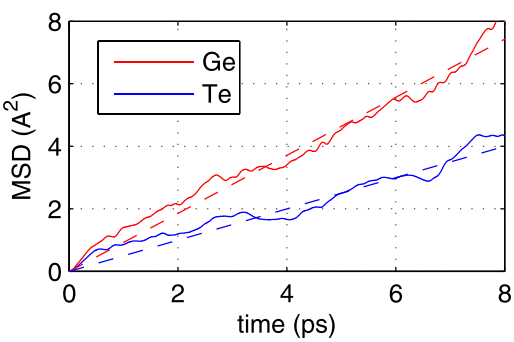


FIG. 5. The MSD of atoms in *a*-GeTe ($T = 800$ K).

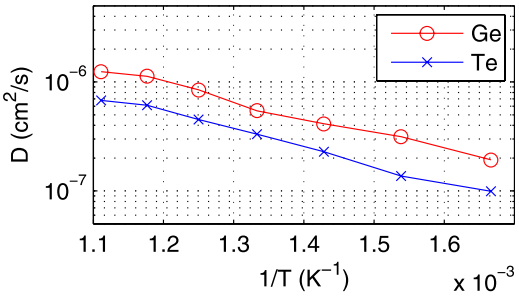


FIG. 6. Temperature dependent diffusivity (D) of atoms in *a*-GeTe.

E. Interfacial energy

The interfacial energy of the interface between *a*-GeTe and *c*-GeTe is computed using

$$\sigma = \frac{E_{ac} - E_a - E_c}{2A}, \tag{8}$$

where $A = l_x l_y$ is the area of the interface between *a*-GeTe and *c*-GeTe in the interface model; E_a, E_c, and E_{ac} are the internal energies of the *a*-GeTe model, the *c*-GeTe model, and the interface model, as shown in Fig. 2. The results for σ are shown in Fig. 7.

When computing the E_a, E_c, and E_{ac}, the periodic boundary conditions are applied at the boundaries of the simulation supercells. As a consequence, the interfacial model actually represents the repeated *a*-GeTe and *c*-GeTe slabs along the *z*-direction. This means that there are two *c*-GeTe/*a*-GeTe interfaces in the supercell of the interfacial model simulations, leading to a factor of 2, as shown in Eq. (8).

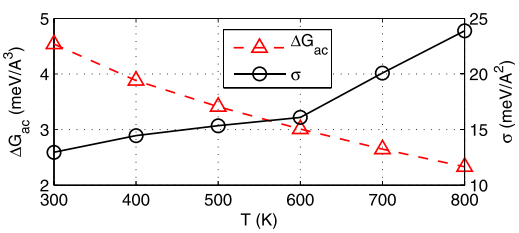


FIG. 7. Gibbs free energy density difference between *a*-GeTe and *c*-GeTe (ΔG_{ac}) and interface energy density (σ).

[This article is copyrighted as indicated in the article. Reuse of AIP content is subject to the terms at: http://scitation.aip.org/termsconditions. Downloaded to] IP: 128.95.215.110 On: Wed, 15 Jan 2014 22:18:00

F. Elastic energy

The elastic energy density E_e of the c-GeTe can be calculated using

$$E_e = \frac{B_0}{B_0'}\left[\frac{1}{B_0'-1}\left(\frac{V_0}{V}\right)^{B_0'} + 1\right] - \frac{B_0}{B_0'-1}\frac{V_0}{V}, \qquad (9)$$

where B_0 (B_0') is the bulk modulus (the derivative of the bulk modulus with respect to pressure) and V (V_0) is the (most energetically favorable) supercell volume.[40] The parameters in Eq. (9) are computed using *ab initio* simulations. First the c-GeTe model is isotropically stretched to different supercell volumes (V). Then the atoms are relaxed using CG to obtain the total energy of the system having the supercell volume V. Finally, the total energy as a function of V is fitted to the Murnaghan equation of state (Fig. 8). The fitting shows that (1) the most energetically favorable lattice constant for c-GeTe is 6.04 Å, which is in decent agreement with the measured value 6.0 Å,[31] (2) the bulk modulus is calculated to be 50.0 GPa, which is in agreement with the values 48.9 GPa (Ref. 41) and 51.0 GPa (Ref. 42) in previous studies, and (3) the derivative of the bulk modulus with respect to pressure is calculated to be 4.62.

Using the simulation results for B_0, B_0', V, and V_0, the elastic energy density is computed using the Murnaghan equation of state (Fig. 8). As shown in Eq. (1) and Fig. 1(a), the elastic energy density (E_e) (and the interfacial energy) opposes the influence of Gibbs free energy density difference (ΔG_{ac}), leading to an increased nucleation energy barrier. As shown in Figs. 7 and 8, E_e is comparable to ΔG_{ac}. Thus, qualitatively speaking, if the contribution of the elastic energy is ignored, nucleation rates will be over-estimated. The quantitative analysis of this tendency will be presented in Secs. III G and III H.

G. Critical nuclei radius and formation energy

Using the simulation results for ΔG_{ac} (Sec. III D), σ (Sec. III E), and E_e (Sec. III F), the calculated nucleation formation energy ΔG (Eq. (1) and Fig. 1) is shown in Fig. 9. The x and y coordinates of the peak of the ΔG curves represent the critical nuclei radius r_c (Fig. 10) and the critical formation energy ΔG_c (Fig. 11), respectively.

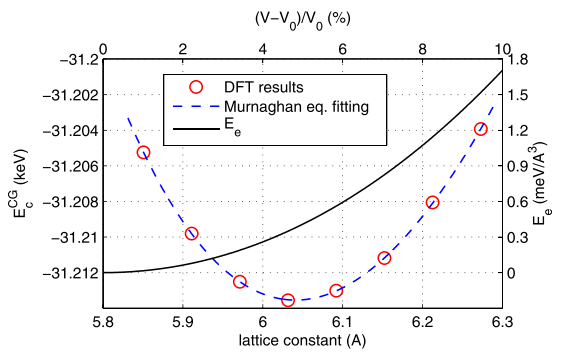


FIG. 8. Total energy of c-GeTe model (E_c^{CG}) under strain (corresponding to different lattice constants), fitted to the Murnaghan equation of state is given by the left-hand/bottom coordinates, and the elastic energy density (E_e) as a function of $(V\text{-}V_0)/V_0$ is given by the right-hand/upper coordinates. V is c-GeTe supercell volume, and V_0 is the most energetically favorable supercell volume of c-GeTe model.

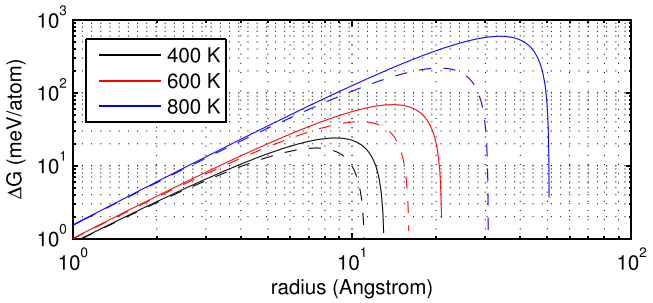


FIG. 9. Formation energy (ΔG) when elastic energy is included (solid lines) and ignored (dashed lines).

Figs. 9–11 show that (1) both ΔG_{ac} and r_c increase monotonously as temperature rises, since the increased thermal vibration tends to break the chemical bonds making nucleation more difficult, and (2) E_e plays an important role in determining ΔG, ΔG_c, and r_c. For $T = 400$, 600, 800 K, ignoring E_e leads to 27.2%, 41.7%, and 63.4% underestimations of ΔG_c, and 14.8%, 23.4%, and 39.5% underestimations of r_c.

H. Nucleation rate and growth speed

The nucleation rate I and the growth rate u are computed from Eqs. (2) and (3) using the values of E_D (Sec. III C), ΔG_{ac} (Sec. III D), and ΔG_c (Sec. III G). The results are shown in Fig. (12) in which normalized nucleation and growth rates I/I_0 and u/u_0 are plotted as a function of temperature. Plotted in this way the results focus on the role of elastic energy and on the temperature-dependence of the nucleation and growth rates. Calculating values of I_0 and u_0 would involve brute-force AIMD simulations, requiring orders of magnitude longer simulation times (about 10^2-10^3 ps).[16–28]

Fig. 12 shows that the nucleation rate (I/I_0 with E_e) peaks at around 600 K. As shown in Eq. (2), this is because atom diffusivity D increases monotonously with temperature (Fig. 6), increasing the nucleation rate I, whereas the critical formation energy barrier ΔG_c (Fig. 11) increases with increasing temperature since ΔG_{ac} decreases making nucleation more difficult. A maximum appears around 600 K. From Fig. 12, if the elastic energy is ignored, I will be significantly overestimated (by 20.8%, 74.2%, and 240.2% when $T = 400$, 600, and 800 K, respectively). This originates from the

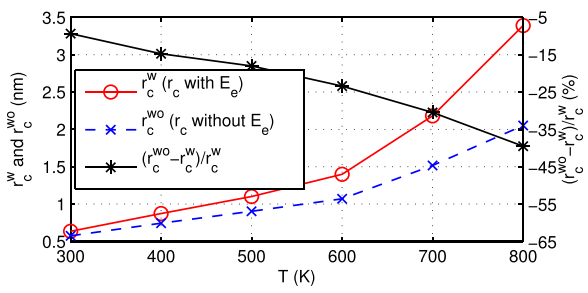


FIG. 10. Critical nuclei radius with elastic energy E_e included (r_c^w) and without E_e (r_c^{wo}).

[This article is copyrighted as indicated in the article. Reuse of AIP content is subject to the terms at: http://scitation.aip.org/termsconditions. Downloaded to] IP: 128.95.215.110 On: Wed, 15 Jan 2014 22:18:00

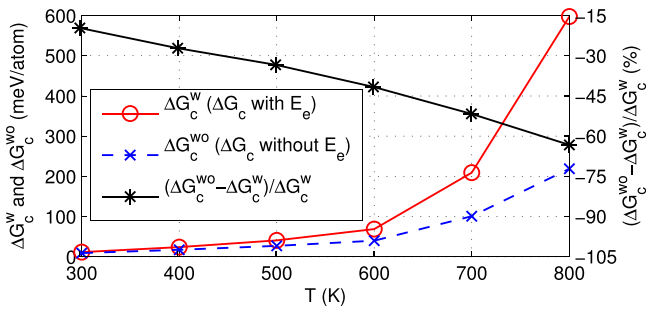


FIG. 11. Critical formation energy with elastic energy E_e included (ΔG_c^w) and without E_e (ΔG_c^{wo}).

underestimation of the critical formation energy barrier (Fig. 11) without elastic effects.

In the temperature range of our interests here, the growth speed u increases as temperature increases, as shown in Fig. 12. According to Eq. (3), u is determined by both the diffusivity D and the Gibbs free energy density difference ΔG_{ac}. When T is low ΔG_{ac} is large, so D, which increases as T increases, largely determines u. When T approaches the melting temperature $T_m = 998$ K, ΔG_{ac} will decrease to a very small value (Fig. 7), which will lead to the decrease of u.

IV. DISCUSSION

Though crystallization of *a*-PCM is very fast, it is slow compared to the amorphization of *c*-PCM. So the SET operation (crystallization) is the rate-limiting factor in phase change memory devices.[1–3] As a two-step process (nucleation and growth), the speed of crystallization is largely limited by nucleation, since the growth speed is very fast (about 10^0–10^1 nm/ns).[17] Our analysis shows that the nucleation rate has the largest value around 600 K. In the design of PCM-based devices, in order to shorten SET operation time, the SET operation current pulse shape should be optimized such that the PCM active region is controlled at this optimal temperature.

Our analysis shows that the elastic energy exerts considerable impacts on the crystallization properties of *a*-PCM by raising the nucleation formation energy barrier. This unfavorable effect deteriorates the recrystallization speed, which is the bottleneck of the speed of PCM-based devices. Predictably, if the elastic energy can be reduced, say by optimizing the chalcogenide stoichiometry and/or doping, the speed of crystallization and the SET operation of the PCM-based devices can be increased. The simulation results show that, when the annealing temperature is 600 K, the critical nuclei radius is roughly 1.4 nm. This means that the crystallization might occur in ultrascaled nanostructures, indicating a promising scaling scenario of PCM-based information storage device technologies.

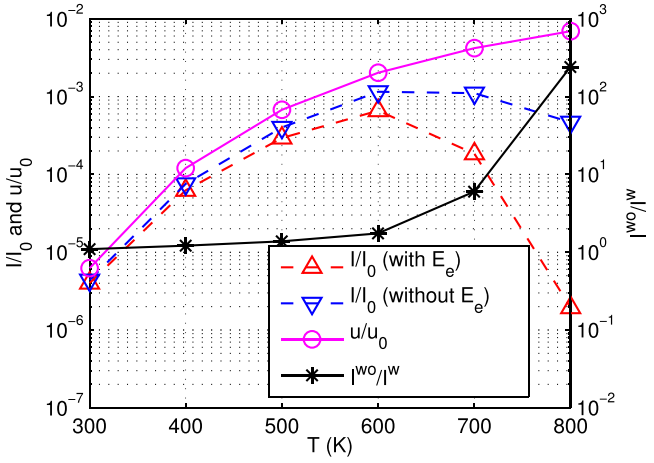


FIG. 12. Normalized nucleation rate I/I_o and growth speed u (the superscript "w"/"wo" means the calculation of I/I_o using Eq. (2) is performed with/without elastic energy E_e).

We note that due to the expensive computational cost of *ab initio* simulations, this paper focuses on homogeneous nucleation and growth of crystals without crystalline anisotropy. Additionally, in real PCM-based devices, different nucleation mechanisms may arise (e.g., heterogeneous nucleation at lower undercooling) due to the presence of additional defects (e.g., interfacial energies, dislocations, grain boundaries, and interfaces between the PCM and the encapsulating materials).[29,43,44] These factors introduce more complexity affecting crystallization kinetics, however these effects are not accounted for here. These effects deserve future investigation. In Fig. 8 and Eq. (9), the elastic energy is computed when the lattice temperature is zero. The temperature dependence of the elastic energy is not addressed in this paper. Also, we would like to mention that only one amorphous sample is used in our analysis, due to the high computational cost to run the *ab initio* simulations on multiple samples. The sample-to-sample variation deserves future research too.[45]

V. CONCLUSION

The temperature dependent crystallization properties of *a*-GeTe are analyzed by combining *ab initio* simulations with macroscopic nucleation and growth theory. We have found that nucleation rates peak at around 600 K. The critical nucleus radius at 600 K is only 1.4 nm, indicating an extremely promising scaling scenario. The importance of elastic energy in crystallization is stressed. It is pointed out that ignoring the elastic energy can lead to 27.2%, 41.7%, and 63.4% underestimations of the critical formation energy barriers, 14.8%, 23.4%, and 39.5% underestimations of the critical nucleus radius and 20.8%, 74.2%, and 240.2% overestimations of the nucleation rate for annealing temperature of 400, 600, and 800 K, respectively.

ACKNOWLEDGMENTS

This work was supported by U.S. National Science Foundation (NSF) under Grant Award 1006182. This work used the Extreme Science and Engineering Discovery Environment (XSEDE), which is supported by National Science Foundation (Grant No. OCI-1053575). This work was facilitated through the use of advanced computational, storage, and networking infrastructure provided by the Hyak supercomputer system, supported in part by the University of Washington's eScience Institute.

[This article is copyrighted as indicated in the article. Reuse of AIP content is subject to the terms at: http://scitation.aip.org/termsconditions. Downloaded to] IP: 128.95.215.110 On: Wed, 15 Jan 2014 22:18:00

[1]*Phase Change Materials Science and Applications*, edited by S. Raoux and M. Wuttig (Springer, New York, 2009).
[2]H. P. Wong, S. Raoux, S. Kim, J. L. Liang, J. P. Reifenberg, B. Rajendran, M. Asheghi, and K. E. Goodson, Proc. IEEE **98**, 2201–2227 (2010).
[3]G. W. Burr, M. J. Breitwisch, M. Franceschini, D. Garetto, K. Gopalakrishnan, B. Jackson, B. Kurdi, C. Lam, L. A. Lastras, A. Padilla, B. Rajendran, S. Raoux, and R. S. Shenoy, J. Vac. Sci. Technol. B **28**, 223 (2010).
[4]W. J. Wang, D. Loke, L. P. Shi, R. Zhao, H. X. Yang, L. T. Law, L. T. Ng, K. G. Lim, Y. C. Yeo, T. C. Chong, and A. L. Lacaita, Nat. Sci. Rep. **2**, 1 (2011).
[5]F. Xiong, A. Liao, D. Estrada, and E. Pop, Science **332**, 568 (2011).
[6]S. W. Nam, H. S. Chung, Y. C. Lo, L. Qi, J. Li, Y. Lu, A. T. C. Johnson, Y. Jung, P. Nukala, and R. Agarwal, Science **336**, 1561 (2012).
[7]D. Loke, T. H. Lee, W. J. Wang, L. P. Shi, R. Zhao, Y. C. Yeo, T. C. Chong, and S. R. Elliott, Science **336**, 1566 (2012).
[8]R. E. Simpson, M. Krbal, P. Fons, A. V. Kolobov, J. Tominaga, T. Uruga, and H. Tanida, Nano Lett. **10**, 414 (2010).
[9]M. A. Caldwell, S. Raoux, R. Y. Wang, H. P. Wong, and D. J. Milliron, J. Mater. Chem. **20**, 1285 (2010).
[10]S. Raoux, J. L. Jordan-Sweet, and A. J. Kellock, J. Appl. Phys. **103**, 114310 (2008).
[11]S. Raoux, C. T. Rettner, J. L. Jordan-Sweet, V. R. Deline, J. B. Philipp, and H. L. Lung, in *Proceedings of European Symposium on Phase Change and Ovonic Science* (2006), p. 127.
[12]H. P. Wong, S. Kim, B. Lee, M. A. Caldwell, J. L. Liang, Y. Wu, R. G. D. Jeyasingh, and S. M. Yu, in 10th IEEE International Conference on Solid-State and Integrated Circuit Technology (2010).
[13]S. Raoux, G. W. Burr, M. J. Breitwisch, C. T. Rettner, Y. C. Chen, R. M. Shelby, M. Salinga, D. Krebs, S. H. Chen, H. L. Lung, and C. H. Lam, IBM J. Res. Dev. **52**, 465–479 (2008).
[14]J. Liu, B. Yu, and M. P. Anantram, IEEE Electron Device Lett. **32**, 1340 (2011).
[15]J. Liu and M. P. Anantram, J. Appl. Phys. **113**, 063711 (2013).
[16]Z. M. Sun, J. Zhou, and R. Ahuja, Phys. Rev. Lett. **98**, 055505 (2007).
[17]Z. M. Sun, J. Zhou, and R. Ahuja, Phys. Rev. Lett. **96**, 055507 (2006).
[18]J. Hegedus and S. R. Elliott, Nat. Mater. **7**, 399 (2008).
[19]M. Krbal, A. V. Kolobov, P. Fons, J. Tominaga, S. R. Elliott, J. Hegedus, and T. Uruga, Phys. Rev. B **83**, 054203 (2011).
[20]T. H. Lee and S. R. Elliott, Phys. Rev. B **84**, 094124 (2011).
[21]T. H. Lee and S. R. Elliott, Phys. Rev. Lett. **107**, 145702 (2011).
[22]J. Akola and R. O. Jones, Phys. Rev. B **76**, 235201 (2007).
[23]J. Akola and R. O. Jones, J. Phys.: Condens. Matter **20**, 465103 (2008).
[24]J. Akola and R. O. Jones, Phys. Rev. Lett. **100**, 205502 (2008).
[25]J. Akola, R. O. Jones, S. Kohara, S. Kimura, K. Kobayashi, M. Takata, T. Matsunaga, R. Kojima, and N. Yamada, Phys. Rev. B **80**, 020201 (2009).
[26]J. Akola and R. O. Jones, Phys. Rev. B **79**, 134118 (2009).
[27]J. Akola, J. Larrucea, and R. O. Jones, Phys. Rev. B **83**, 094113 (2011).
[28]J. Kalikka, J. Akola, J. Larrucea, and R. O. Jones, Phys. Rev. B **86**, 144113 (2012).
[29]J. W. Christian, *The Theory of Transformations in Metals and Alloys* (Elsevier Science Ltd., Oxford, UK, 2009).
[30]T. Nonaka, G. Ohbayashi, Y. Toriumi, Y. Mori, and H. Hashimoto, Thin Solid Films **370**, 258 (2000).
[31]T. Chattopadhyay, J. X. Boucherle, and H. G. Schnering, J. Phys. C **20**, 1431 (1987).
[32]G. E. Ghezzi, Appl. Phys. Lett. **99**, 151906 (2011).
[33]D. B. Dove, M. B. Heritage, K. L. Chopra, and S. K. Bahl, Appl. Phys. Lett. **16**, 138 (1970).
[34]S. Nose, J. Chem. Phys. **81**, 511 (1984).
[35]M. Parrinello and A. Rahman, Phys. Rev. Lett. **45**, 1196 (1980).
[36]J. M. Soler, E. Artacho, J. D. Gale, A. Garca, J. Junquera, P. Ordejon, and D. Sanchez-Portal, J. Phys.: Condens. Matter **14**, 2745 (2002).
[37]J. P. Perdew, K. Burke, and M. Ernzerhof, Phys. Rev. Lett. **77**, 3865 (1996).
[38]K. C. Mills, *Thermodynamic Data for Inorganic Sulphides, Selenides and Tellurides* (Butterworth-Heinemann Ltd., London, UK, 1974).
[39]R. F. Brebrick, J. Chem. Phys. **41**, 1140 (1964).
[40]F. D. Murnaghan, Proc. Natl. Acad. Sci. **30**, 244 (1944).
[41]C. M. I. Okoye, J. Phys.: Condens. Matter **14**, 8625 (2002).
[42]K. M. Rabe and J. D. Joannopoulos, Phys. Rev. B **36**, 3319 (1987).
[43]H. I. Aaronson, G. Spanos, R. A. Masamura, R. G. Vardiman, D. W. Moon, E. S. K. Menon, and M. G. Hall, Mater. Sci. Eng.: B **32**, 107 (1995).
[44]J. Liu, B. Yu, and M. P. Anantram, in *2011 11th IEEE International Conference on Nanotechnology, Portland, Oregon, USA* (2011), pp. 1343–1347.
[45]See supplementary material at http://dx.doi.org/10.1063/1.4861721 for atomic coordinates of the simulation models and the time-dependent fluctuations of the pressure, mass density, internal energy, and temperature.

[This article is copyrighted as indicated in the article. Reuse of AIP content is subject to the terms at: http://scitation.aip.org/termsconditions. Downloaded to] IP: 128.95.215.110 On: Wed, 15 Jan 2014 22:18:00